Check for updates

ASME Journal of Thermal Science and Engineering Applications
Online journal at:
https://asmedigitalcollection.asme.org/thermalscienceapplication

An In-Depth Comparison of Straight and Wavy Microchannel Heat Exchangers

Vishwas Kumar Pandey[1]
Department of Mechanical Engineering,
Birla Institute of Technology and Science Pilani,
Pilani Campus,
Pilani, Rajasthan 333031, India
e-mail: p20210516@pilani.bits-pilani.ac.in

Vinay Pratap Singh Negi
Department of Mechanical Engineering,
Birla Institute of Technology and Science Pilani,
Pilani Campus,
Pilani, Rajasthan 333031, India
e-mail: p20210456@pilani.bits-pilani.ac.in

Chennu Ranganayakulu
Department of Mechanical Engineering,
Birla Institute of Technology and Science Pilani,
Pilani Campus,
Pilani, Rajasthan 333031, India
e-mail: c.ranganayakulu@pilani.bits-pilani.ac.in

This paper presents extensive fluid flow and Heat-Transfer studies conducted using a commercial computational fluid dynamics (CFD) package known as CFD-ACE® to elaborate and expand on the reference studies available for ceramic-compact counterflow microchannel heat exchangers (MCHEs). The computational 3D model was developed using an experimentally tested MCHE and validated with experimental data with 3–5% variation for hot fluid and 6–12% variation for cold fluid for the entire design of experiments (DoEs). This study aimed to identify the performance of novel microchannel shapes using numerical analysis. The MCHE has good heat exchange properties, a compact design at industrial throughput, and a lower inner volume. During the study and identification of novel channel shapes, the segmented wavy MCHE was evaluated. The results were compared with those of the same volume and area straight MCHE baseline design under various identical operating conditions. Although the performance in terms of effectiveness is increased up to ∼12–25% in wavy MCHE with respect to straight MCHE simultaneously, the pressure drop is also increased by ∼60–80% under the same operating conditions. Therefore, performance and trade-offs are required to make the correct decision regarding feasibility. The effectiveness of the heat-transfer enhancement was also evaluated by plotting the heat-transfer coefficient ratio with respect to the pressure ratio of the two designs under identical operating conditions. This numerical study clearly indicates that wavy channels are better from the thermal performance point of view, whereas straight channels are better from the pumping power point of view, and the quantitative values are presented in graphical form.
[DOI: 10.1115/1.4064985]

Keywords: straight channel micro heat exchanger, MCHE, wavy channel microheat exchanger, friction factor, j factor calculation., conduction, forced convection, heat and mass transfer, heat exchangers, heat-transfer enhancement, micro/nanoscale heat transfer

1 Introduction

Microchannel heat exchangers (MCHEs) are being used in an increasing number of ways every day as people look for faster and more efficient ways to transfer heat. Microelectromechanical systems (MEMS)-based MCHEs are becoming more popular in the medical, electronics, and aerospace industries because they are good at transferring heat, can be made sufficiently small for industrial use, and have less space inside them. MCHE applications are identified in almost all areas or fields; however, a few application field examples are subsequently discussed to understand how requirements change with time. These requirements are pushing engineers to investigate solutions that meet the expectations of consumers. In the power generation industry, the demand for small-scale power plants, such as micro-scale power plants, is increasing as new working fluid carbon dioxide (CO_2), which can operate in a supercritical regime, is identified. These plants are known as supercritical CO_2 Brayton cycle (SCBC) micropower plants. Supercritical CO_2-based Brayton cycle power plants have higher efficiency than conventional steam power plants [1]. Owing to their increased efficiency and compactness, closed Brayton supercritical CO_2 power cycles are a viable solution for waste heat bottoming cycles compared with Rankine steam bottoming cycles [2].

Additionally, microchannel evaporators and condensers, which are both small and lightweight, are required. Microchannel evaporators/condensers are used in compact refrigeration systems; by decreasing the amount of refrigerant charge, the systems help mitigate the effects of warming the planet and depleting the ozone layer. The International Technology Roadmap of Semiconductors (ITRS 2011) expected that the power dissipation would exceed 800 W by 2026 (the predicted value for 2015 was approximately 270 W) from a microprocessor chip; for example, the value of heat dissipation reached 240 W for the ORACLE SPARC T4 processor in 2011 for high-performance computers. The typical die size of the ORACLE SPARC T4 processor is around 403 mm^2, which means the heat flux value is about 0.6 MW/m^2 [3]. Similarly, every air force is looking for the most efficient, accurate, and better-featured aircraft on the defense side. However, more power is consumed when using more features and cruising with a higher Mach

[1]Corresponding author.

Manuscript received October 15, 2023; final manuscript received February 22, 2024; published online March 18, 2024. Assoc. Editor: Mark Ricklick.

Copyright © 2024 by ASME

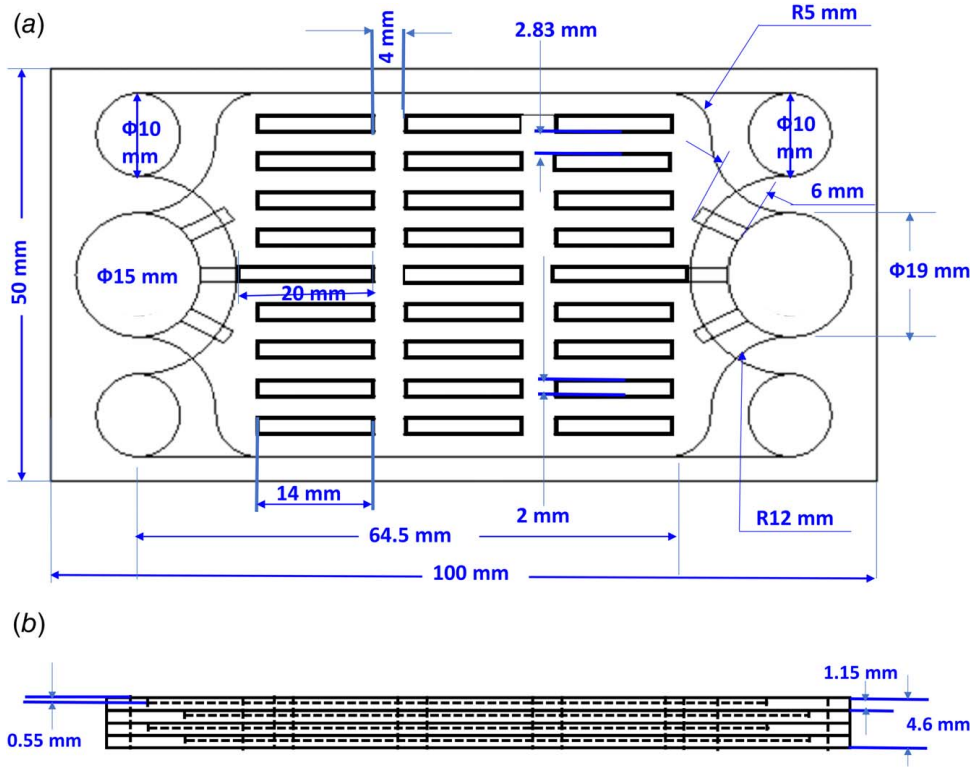

Fig. 1 (*a*) Plate drawing and dimension and (*b*) thickness of full stack and each plate

Number. To fulfill these needs, technologists and engineers must come up with a solution to achieve very efficient heat transfer to meet lightweight and compact size constraints, and there is a significant demand for MCHE. The efficiency of an MCHE is largely determined by its microchannel geometry and flow volume [4].

2 Computational Model of Existing MCHE

Karayiannis and Mahmoud [3] discussed the importance of flow boiling in microchannels for cooling at the computer-chip level. This paper also describes the complex phenomenon of flow boiling and several fundamental issues such as flow instability and nucleation. Microchannel counterflow heat exchangers using alumina as the material and water as the working fluid were designed and fabricated by Alm et al. [5], and their low-temperature performance was evaluated. It is well known that longitudinal conduction within solid materials can play an important role in the performance, particularly in small high-performance counterflow heat exchangers. Although textbooks provide a general formulation of longitudinal conduction [6], more thorough analyses can be attained by simulating the fluid flow and conjugate heat transfer in three dimensions [7,8]. In a highly efficient counterflow MCHE, the selection of a solid material plays a vital role in longitudinal conduction because longitudinal conduction should be within the material. However, several correlations and formulations for longitudinal conduction [9,10] and conjugate heat transfer are available in various literatures [11–13]. Kumar et al. [4] briefly discussed the effect of different materials on the performance and pressure drop under the same operating conditions with water as the liquid coolant for electronic device heatsinks. Sheth et al. [14] compared the performance of an MCHE with that of a conventional X-38 liquid-to-liquid heat exchanger for spacecraft applications. From this study, it was observed that the MCHE provided approximately 20% more heat-transfer rate, but it also provided the requirement of high pumping power owing to almost 80% more pressure drop requirements. Kee et al. [6] numerically simulated a counterflow ceramic sensible cooling (Air to Air) MCHE. A couple of experimental datasets are available in this work, along with geometrical details, and these data will be used as a reference for numerical data validation. Micro-electro-mechanical system-based heat exchangers for cooling microchips were designed by Ionescu and Neagu [7] using a variety of geometrical shapes (circular, rhombic, square, and orthogonal) to meet the increasingly cramped space requirements determined using the Finite Element Method. Hasan et al. [15] investigated how the geometry of the channels (circle, square, rectangular, iso-triangular, and trapezoidal cross sections) affected the efficiency of a balanced counterflow MCHE with 16 channels (eight channels for each of the fluids). This study shows that, for a given heat exchanger volume, increasing the number of channels improves both the effectiveness (ε) and ΔP. Regarding boiling flow in microchannels, Kumar et al. [4] analyzed the most recent research available from 2000 onwards. An in-depth review of the flow patterns formed and the parameters

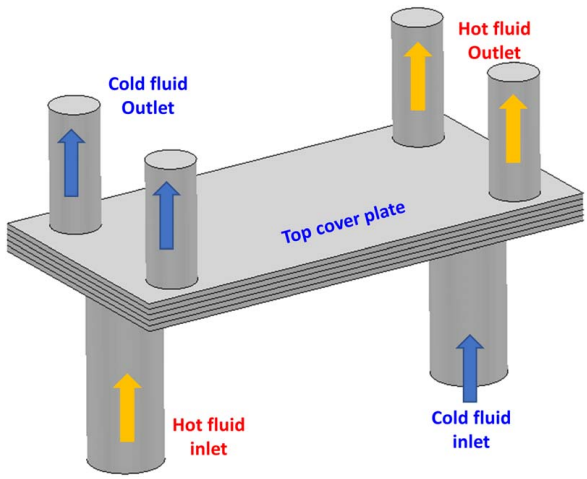

Fig. 2 Computational domain with inlet and outlet pipes [6]

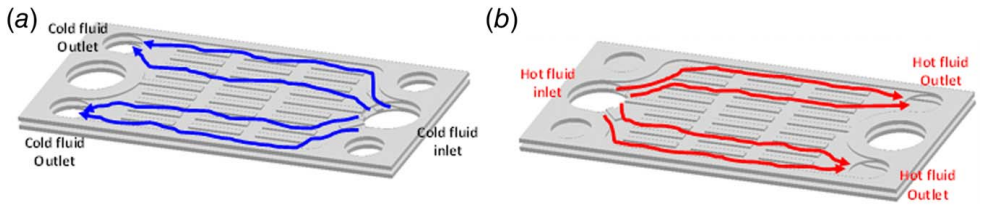

Fig. 3 Flow arrangement in hot and cold plates in MCHE [6]

influencing the flow pattern transitions during multiphase heat transfer in micro- or mini-channels was presented. Boiling flow in microchannels/devices with varying difficulties: flow regimes, flow pattern maps, and modeling approaches.

When discussing numerical modeling, Shakir et al. [16] focused on the molecular or transition regime rather than the continuum. Typically, the flow regime is determined by the Knudsen number (Kn). When Kn is small ($Kn \leq 0.001$), the fluid is in a continuous state, but when it is large, say ($Kn \leq 10$), free molecular flow is assumed. In this study, we focus on the transition flow region for Knudsen numbers in the range of $0.001 \leq Kn \leq 0.1$. Using the finite element method, Ranganayakulu et al. [8,17] discussed the impact of longitudinal heat conduction on compact tube-fin heat exchangers. This study found that incorporating the effects of longitudinal conduction and non-uniform flow and temperature distribution into the analysis significantly degrades the performance of compact heat exchangers compared with not including these factors. A numerical method for modeling a crossflow compact heat exchanger was discussed by Chennu [18]. The author also discussed ΔP in small heat exchanger tubes and fins as well as single-phase steady-state heat transfer. In this study, several charts were created for several different fin configurations, including square and triangular fins (both perforated and unperforated), offset strip fins, and wavy fins. Jegan et al. [19] investigated that small change in the tube shape by introducing rifle in experiment and concluded that rifle really helped in enhancement of heat transfer even at low pressure due to strong swirling flow.

3 Existing MCHE Experimental and Simulation Models

3.1 Model Description. Building an analysis methodology and gaining confidence in the approach requires experimental validation of the results from computational models. We began by using computational fluid dynamics (CFD) to verify the 2011 experimental work by Kee et al. Therefore, a computational 3D model of the MCHE was built using CFD-ACE®, which has been manufactured and experimentally tested in previous studies and the details of the experimental setup are provided in a previous study [6]. Microchannel heat exchangers (MCHEs) with a flow layer of 50 mm × 100 mm and made of ceramics are shown in Fig. 1. Ten microchannels measuring 550 μm in height and 2.8 mm in width were placed in the flow layer. The two streams coming from the hot and cold channels were divided by a plate 600 μm thick. Each microchannel column and row were separated by 4 mm and 2.83 mm respectively. There was a total of four alumina flow layers in the MCHE design and construction, two of which were heated and the other two were cooled.

The primary purpose of the gap between the two columns was to enable an equal pressure distribution in the columns. It is evident that the axial pressure drop is inversely proportional to the cube of the channel height, and even small differences in the geometry significantly affect the flow variation between the microchannels. This proves that the gap tends to improve the flow distribution. Another purpose of this gap is to reduce the longitudinal wall conduction, which degrades the performance of the MCHE. Another benefit of the gap between the columns is that it helps break the boundary layer at the end of each channel, which provides local entry-length boundary layer behaviors, which is favorable for improving the local heat-transfer coefficient.

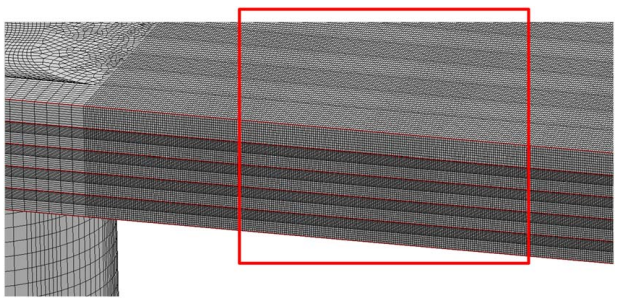

Fig. 4 Gridded model of computationally tested MCHE

Table 1 Grid points and cell counts of various computed MCHE model

S. No.	Description	Mesh counting	
		Nodes	Cells
1	Fine Mesh_04	12211980	10609674
2	Fine Mesh_03	11168764	9573402
3	Fine Mesh_02	10048660	8537130
4	Fine Mesh_01	9063736	7715826
5	Optimum Mesh	7988488	6819858
6	Coarse Mesh_01	6390118	5414142
7	Coarse Mesh_02	5652502	4808670
8	Coarse Mesh_03	4784650	4095078
9	Coarse Mesh_04	4223770	3572886

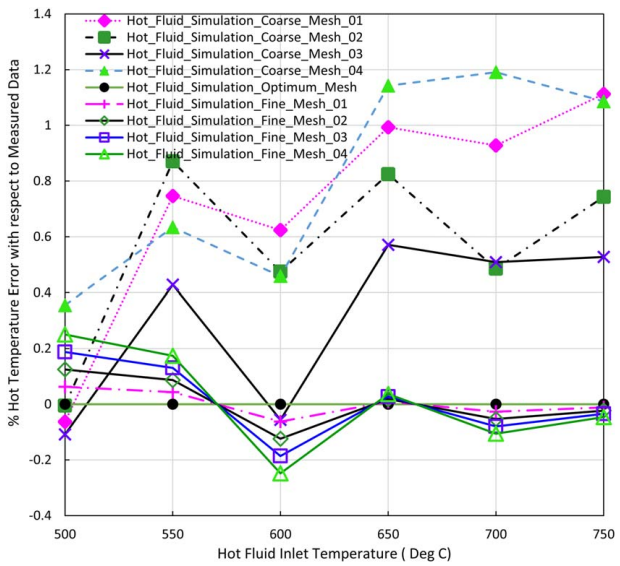

Fig. 5 The percentage change in hot-fluid outlet temperature with different grid models

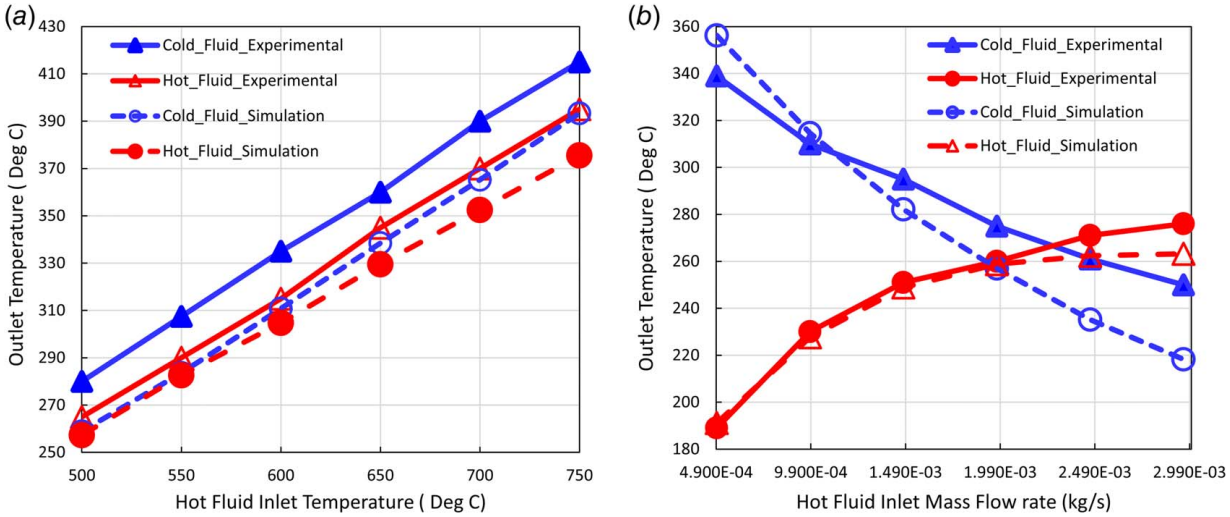

Fig. 6 Experimental versus predicted outlet temperatures for hot and cold fluids: (*a*) hot-fluid inlet temperature effect and (*b*) balanced flow effect

Figure 2 depicts the computational domain with inlet and outlet pipes, with hot and cold fluids entering through the center hole located at the bottom and leaving through the two outlet holes at the top. All the layers of internal flow are the same, with the only difference being the rotation of 180 deg between adjacent layers. The use of parallel layers is motivated by the need to reduce production costs.

A cold plate comes into contact with a cold fluid, whereas a hot plate comes into contact with a hot fluid. The computational model examined a set of four plates, two hot and two cold, by rearranging their positions. As shown in Fig. 3(*a*), the cold fluid entered the unit from the right and exited from the left. In a counterflow arrangement, the hot fluid enters the left and exits to the right, with the goal of maximizing heat transfer as shown in Fig. 3(*b*). The computational model was built in CFD-GEOM® and analyzed in CFD-ACE® as per the reference study. The assembly has one inlet and two outlet manifolds for each fluid. The MCHE was built of alumina material, and air was used as a heat-transfer medium for the reference study.

A detailed Design of Experiments (DoE) was carried out by varying the hot-fluid temperature and mass flow changes in balanced and unbalanced ways, while keeping all other parameters constant. DoE points and boundary conditions were used, as in reference studies [6], to validate the computational model using experimental data. Moreover, alumina was used as the material for the MCHE.

To understand the effect of the material on MCHE performance, a detailed study was conducted in which the MCHE material was changed from Alumina to Stainless Steel (SST), Silicon, Graphite, and Copper independently for the entire DoE range.

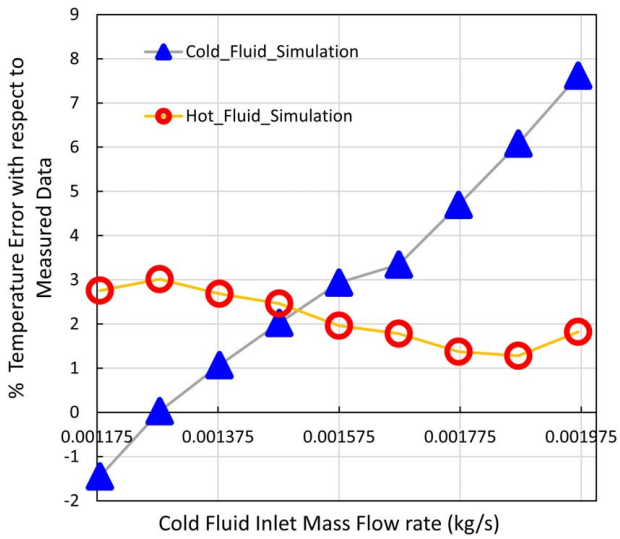

Fig. 7 The percentage error in predicted outlet temperatures for hot and cold fluids

3.2 Governing Equations. A commercial CFD-ACE® package was used in this study. For researchers, it is essential to know what is happening in the commercial code background while solving the problem. Proper velocity and temperature profiles in the computational domain were obtained by solving the continuity, momentum, and energy equations. The continuity, momentum, and energy conservation equations are as follows:

3.2.1 Continuity Equation

$$\frac{D\rho}{Dt} + \rho \frac{\partial U_i}{\partial x_i} = 0 \tag{1}$$

3.2.2 Momentum Equation

$$\underbrace{\rho \frac{\partial U_j}{\partial t}}_{A_1} + \underbrace{\rho U_i \frac{\partial U_j}{\partial x_i}}_{B_1} = \underbrace{-\frac{\partial P}{\partial x_j}}_{C_1} \underbrace{-\frac{\partial \tau_{ij}}{\partial x_i}}_{D_1} + \underbrace{\rho g_j}_{E_1} \tag{2}$$

where,

$$\tau_{ij} = -\mu\left(\frac{\partial U_j}{\partial x_i} + \frac{\partial U_i}{\partial x_j}\right) + \frac{2}{3}\delta_{ij}\mu \frac{\partial U_k}{\partial x_k} \tag{3}$$

Here, A_1 is the local change with time, B_1 is the convective momentum exchange, C_1 is the surface force, D_1 is the diffusion momentum exchange, and E_1 is the mass force

3.2.3 Energy Equation

$$\underbrace{\rho c_\mu \frac{\partial T}{\partial t}}_{I} + \rho c_\mu \underbrace{U_i \frac{\partial T}{\partial x_i}}_{II} = \underbrace{-P \frac{\partial U_i}{\partial x_i}}_{III} + \underbrace{\lambda \frac{\partial^2 T}{\partial x_i^2}}_{IV} \underbrace{-\tau_{ij} \frac{\partial U_j}{\partial x_i}}_{V} \tag{4}$$

where I is the local energy changes with time, II is the convective term, III is the pressure work, IV is the heat flux (Diffusion), and V

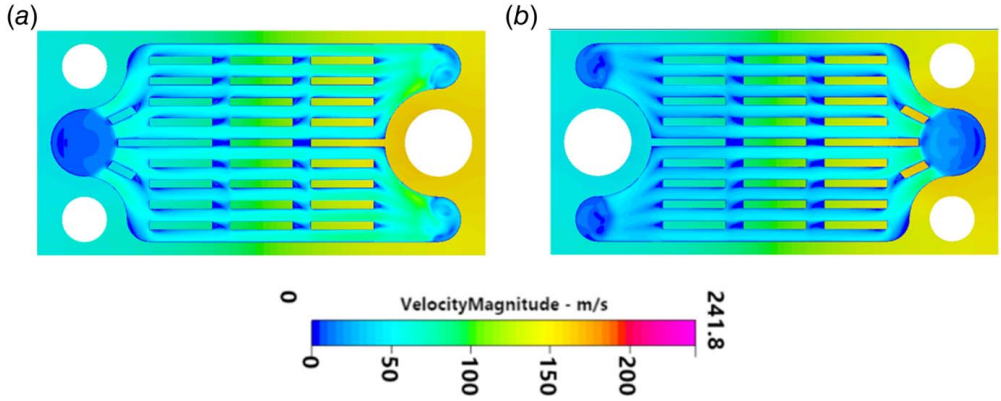

Fig. 8 Velocity profile for hot and cold fluids: (*a*) cold fluid and (*b*) hot fluid

is the Irreversible transfer of mechanical energy into heat. The continuity and momentum equations can be resolved if the fluid is compressible.

3.3 Grid Generation and Mesh Independence Test. The accuracy of the computational model depends on the discretization of the problem and the physics involved. In the discretization of the problem, a proper mesh or grid must be created to capture the correct behavior or trends. Therefore, both the element size and number matter significantly. Recall that if the grid size is smaller than required, it will increase the number of grid points. These extra grid points increase the computation time and delay in obtaining the results without any additional benefits. On the other hand, if grid points or the number of grids is not sufficient, then the accuracy of the results will be questioned and may lead to incorrect conclusions. Therefore, the grid optimization or grid independence test is an essential step and must be executed before further analyzing the model for all required operating conditions.

In this study, a grid independence test has been carried out, where the mesh count has increased from 3.5 M to 10.6 M to see the impact of several grid points on results, as shown in Fig. 4 and Table 1.

Multiple cases are analyzed of all different grid numbers computational models, as mentioned in Table 1, to ensure that results and trends are consistent for the entire Design of the Experiment (DoE). For the grid independence test, DoE was performed, in which the hot-fluid temperature was varied from 500 °C to 750 °C with an increase of 50 °C, keeping the rest of the parameter constant.

The temperature drop in the hot fluid was obtained as the output from the computational model for each case. The percentage change in the hot-fluid exit temperature at the outlet with respect to the optimum mesh count was plotted against the inlet hot-fluid temperature for the computational model listed in Table 1. It is concluded that with any further increase in the mesh count from the optimum count model, the impact of the hot fluid's outlet temperature is limited to less than 2%, as shown in Fig. 5.

Therefore, the optimum mesh model with a mesh count of 6.82 M was used for all further validation and prediction studies during the DoE.

3.4 Boundary Conditions. The performance of the MCHE was evaluated experimentally for the following scenarios in the past in published literature [6], and the same boundary conditions were simulated in the numerical analysis as follows:

(a) Hot-fluid inlet temperature DoE: Here, the effect of changing the inlet temperature of the hot fluid from 500 °C to 750 °C was examined, while maintaining the inlet temperature of the cold fluid at a constant 40 °C and an airflow rate of 0.0197 kg/s in both the hot and cold sections of the experiment. The effect of the hot-fluid inlet temperature was studied, and the temperatures of the cold and hot fluids at their respective outlets were measured. When the hot-fluid temperature was increased from 500 °C to 750 °C while keeping all other parameters constant, the temperatures of the cold and hot fluids also increased owing to the higher energy heat exchange.

(b) Balanced flow DoE: This effect is known as "balanced flow" because the mass flowrates of both the hot and cold fluids are changed simultaneously and in such a way that they remain identical relative to one another. Hot and cold fluids entered the system at different but stable inlet temperatures. In this

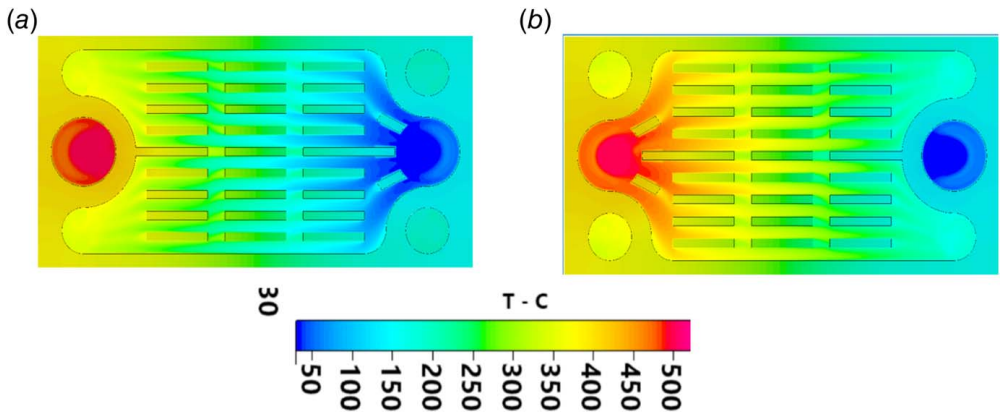

Fig. 9 Temperature profile for hot and cold fluids: (*a*) cold fluid and (*b*) hot fluid

investigation, the inlet temperatures of the hot and cold fluids were held constant at 500 °C and 40 °C, respectively, while the mass flowrates were varied from 0.00493 kg/s to 0.002958 kg/s in increments of 0.00493 kg/s.

(c) Unbalanced flow DoE: The unbalanced flow effect occurs when the mass flowrates of the hot and cold fluids are changed independently of one or both fluids, such that the mass flowrates of both fluids are always different. However, the study maintained a constant difference between the inlet temperatures of hot and cold fluids. In this investigation, the inlet hot and cold fluid temperatures were set to 700 °C and 50 °C, respectively, and the cold fluid mass flowrate was varied from 0.00118 kg/s to 0.00197 kg/s, while the hot-fluid mass flowrate was held constant at 0.00158 kg/s.

3.5 Validation With Results Discussion. The performance of the MCHE was evaluated using a computational model created in CFD-GEOM® and analyzed in CFD-ACE® for all scenarios mentioned in the boundary condition section. The results of the computational model were post-processed using CFD-VIEW®. The thermal and velocity contours were plotted in the hot and cold plate sections along the flow direction. These contours act as virtual sensors for understanding the phenomena and outcomes of the MCHE. The effectiveness of the MCHE is determined by measuring the temperatures of the hot and cold fluids at the outlet of the system, which is a result of postprocessing. When comparing the computed results to the observed experimental data published in the literature [6] regarding the outlet temperatures of hot and cold fluids, the following conclusions were drawn:

(a) Hot-fluid inlet temperature effect: When this scenario was studied through a computational model of the experimentally tested published hardware of the MCHE in the literature with identical boundary conditions, it was concluded that the computed results were in good agreement with the experimental data qualitatively and quantitatively, as shown in Fig. 6, in terms of the outlet temperatures. The percentage differences in the computed outlet temperatures were within 5% and 8% variation for hot and cold fluids, respectively, with respect to the experimental data for the entire range.

From Fig. 6(*a*), it was concluded that the prediction of the hot-fluid outlet temperature was always better than that of the cold fluid; that is, the accuracy of the prediction of the hot fluid was higher than that of the cold fluid. However, when we investigated the geometry, we could say that the hot and cold fluid sections, including all piping, were identical. Because an identical mesh was used here for the hot and cold plate sections, including the piping, it was difficult to believe that the accuracy of the outlet temperature of the cold fluid was lower than that of the hot fluid. However, there might be another possibility that the thermocouple associated with the outlet of the cold fluid side might have lost calibration while testing at the outlet location.

(b) Balanced flow effect: When the balanced flow scenario was studied using the same computational model of the experimentally tested published hardware of the MCHE in the literature with identical boundary conditions, it was concluded that the computed results were very close to the experimental data, as shown in Fig. 6(*b*). The percentage difference in the computed outlet temperatures was within 5% and 12% for hot and cold fluids, respectively, with respect to the experimental data as shown in Fig. 7.

From the velocity contour in the flow channel, it was also concluded that the velocity of the hot fluid decreased from the inlet to the outlet as the density increased with a decrease in temperature owing to the energy heat exchange between the hot and cold fluids, and vice versa for the cold fluid, as in Fig. 8.

Similarly, from the temperature contour of the fluid in the channel, it was also concluded that the cold fluid started picking heat along the flow direction from the hot fluid as it moved from the inlet to the outlet and vice versa for the hot fluid, as shown in Fig. 9.

(c) Unbalanced flow effect: When an unbalanced flow scenario was studied using the same computational model of the experimentally tested published hardware of the MCHE in the literature with identical boundary conditions, it was concluded that the computed results were in good agreement with the experimental data, as shown in Fig. 10. The percentage differences in the computed outlet temperatures were within 5% and 12% for hot and cold fluids, respectively, with respect to the experimental data for the entire range.

3.6 Longitudinal Conduction Effect With Results Discussion. It was evident that the MCHE should be made of less longitudinal conducting material to avoid direct heat loss between the inlet ports of the hot and cold fluids. However, a very high thermal conductivity was recommended in the lateral direction because it helped transfer heat efficiently across the plate from one fluid to another. This implies that less heat was

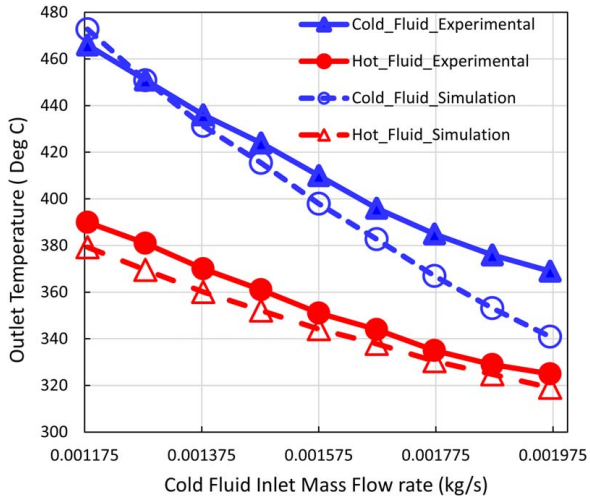

Fig. 10 Experimental versus predicted outlet temperatures for hot and cold fluids

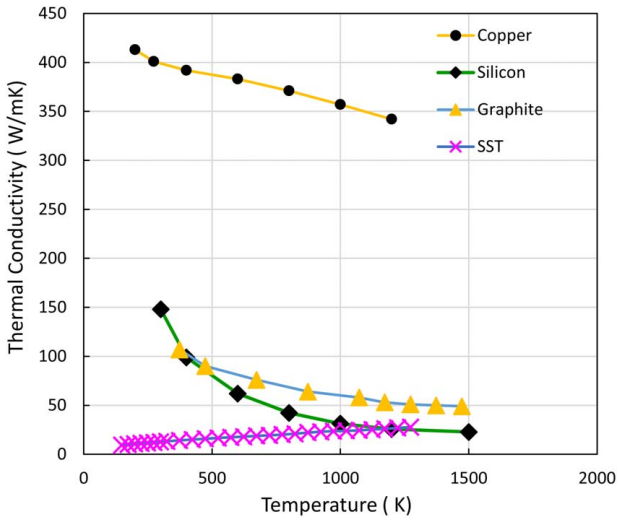

Fig. 11 Thermal conductivity versus temperature for various materials

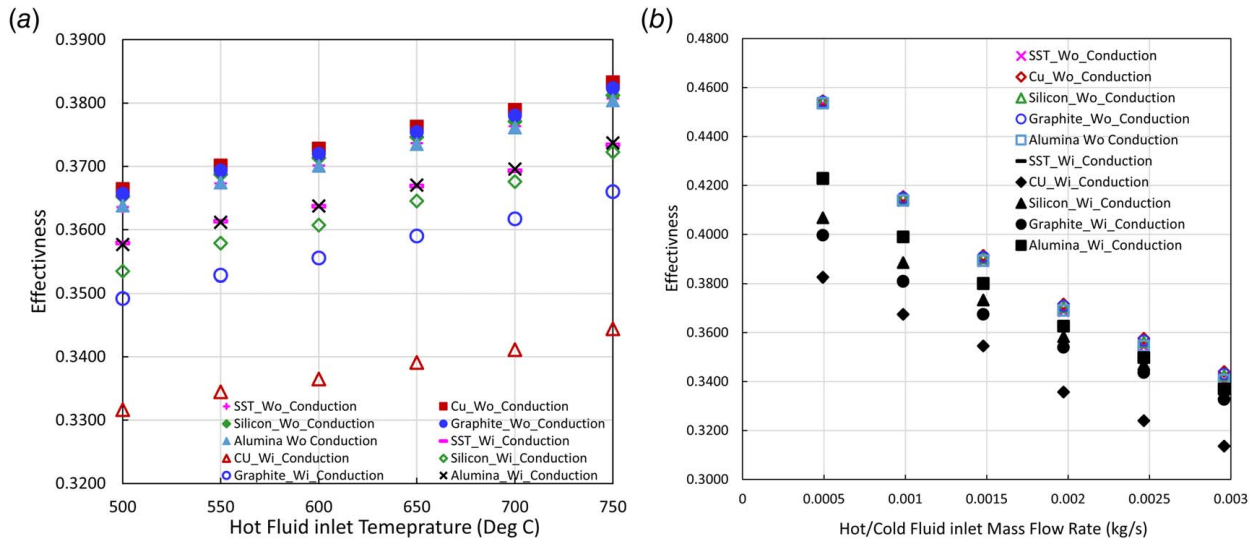

Fig. 12 MCHE effectiveness variation due to longitudinal conduction: (*a*) hot-fluid inlet temperature effect and (*b*) balanced flow effect

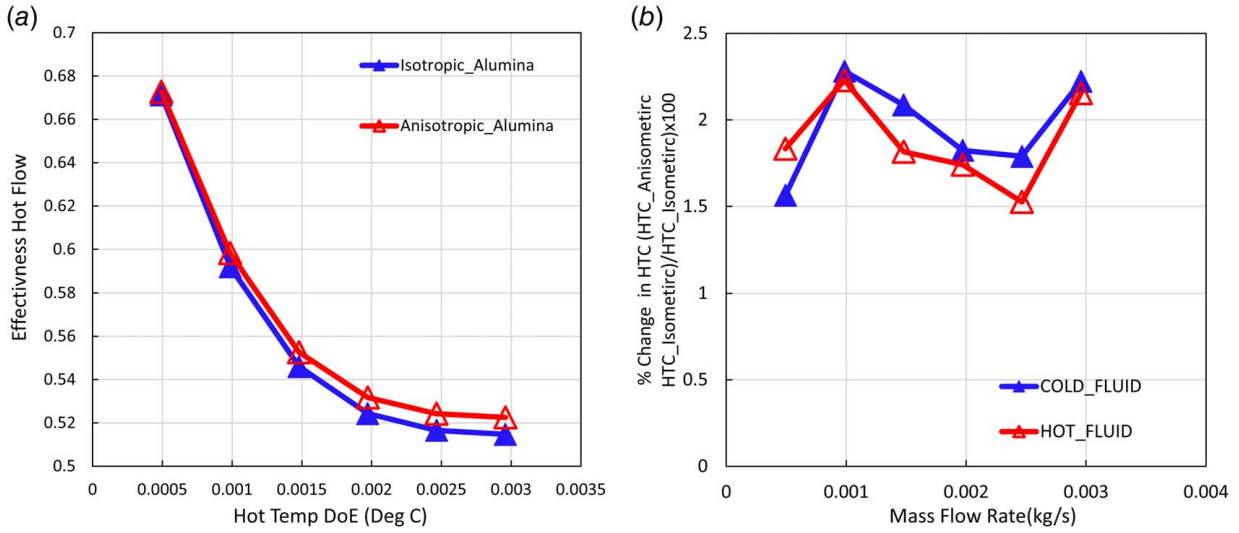

Fig. 13 Isotropic and anisotropic (hypothetical) alumina MCHE: (*a*) effectiveness and (*b*) HTC improvement

lost across the plate. However, a low thermal conductivity is preferred along the flow direction because a high thermal conductivity along the flow direction reduces the effectiveness of the MCHE. These high longitudinal conducting materials increased the dominance of the conduction mode of heat transfer between the inlet and outlet ports, instead of the desirable forced convection.

To virtually study the longitudinal conduction effect using the computational model in the MCHE, the material was changed from Alumina to SST, Silicon, Graphite, and Copper independently. The variations in the thermal conductivity with respect to temperature for SST, Silicon, Graphite, and Copper are shown in Fig 11.

The performance of the MCHE was re-evaluated when the material was changed from Alumina to SST, Silicon, Graphite, and Copper independently for the entire set of DoEs, as described in the section on boundary conditions.

For each scenario, the hot and cold outlet temperatures were obtained from the computational model, which was used to calculate the effectiveness (ε) of the MCHE for the respective conditions using the general equation for the number of transfer units (NTU).

The following procedure was followed to calculate NTU, ε, and the dimensionless longitudinal conduction parameter (λ), considering the thermal conductivity in the longitudinal direction:

(1) The total thermal resistance was determined by calculating the conductance UA between hot and cold streams.

$$\left(\frac{1}{UA}\right) = \left[\left(\frac{1}{h_{\text{hot}}A_s}\right) + \left(\frac{1}{k_{\text{wall}}A_s}\right) + \left(\frac{1}{h_{\text{cold}}A_s}\right)\right] \tag{5}$$

where k_{wall} is the thermal conductivity of wall (W/m · K), A_s is the convective surface area (m^2), h_{hot} is the heat-transfer coefficient (HTC) of hot fluid (W/m^2K), and h_{cold} is the heat-transfer coefficient (HTC) of cold fluid (W/m^2K).

(2) Calculate the number of transfer units for MCHE

$$\text{NTU} = \frac{UA}{C_{\min}} \tag{6}$$

where $C_{\min}$ is the minimum total heat capacity of the fluid.

(3) Calculate dimensionless longitudinal conduction parameter (λ)

$$\lambda = \frac{k_{\text{wall}}\, A_c}{LC_{\min}} \tag{7}$$

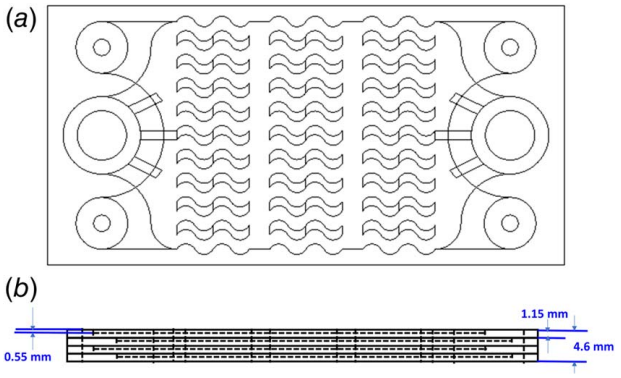

Fig. 14 (*a*) Wavy channel MCHE and (*b*) thickness of full stack and each plate

where A_c is the longitudinal conduction cross-sectional area (m^2); L is the distance between two inlet ports for hot and cold fluids (m).

(4) Calculate effectiveness for counterflow heat exchanger considering longitudinal conduction [6]

$$\varepsilon = 1 - \frac{1}{\left[1 + \mathrm{NTU}\left(\frac{1+\lambda\Phi}{1+\lambda\mathrm{NTU}}\right)\right]} \tag{8}$$

Alternatively, ineffectiveness ($\acute{\varepsilon}$) can be calculated by rearranging the aforementioned equation as follows [6]:

$$\acute{\varepsilon} = (1-\varepsilon) = \frac{1}{\left[1 + \mathrm{NTU}\left(\frac{1+\lambda\Phi}{1+\lambda\mathrm{NTU}}\right)\right]} \tag{9}$$

where,

$$\Phi = \left(\frac{\lambda\mathrm{NTU}}{1+\lambda\mathrm{NTU}}\right)^{1/2} \tag{10}$$

(5) Calculate the effectiveness without considering the longitudinal conduction using $\lambda = 0$ in the equation discussed in *Step 4*. Therefore, a new effectiveness equation can be written without considering longitudinal conduction.

$$\varepsilon = \frac{\mathrm{NTU}}{[1+\mathrm{NTU}]} \tag{11}$$

The results are plotted between λ and ineffectiveness ($\acute{\varepsilon}$). The following conclusions were drawn on the effectiveness of the MCHE owing to the longitudinal conduction effect on the entire DoE set, as discussed in Sec. 3.5:

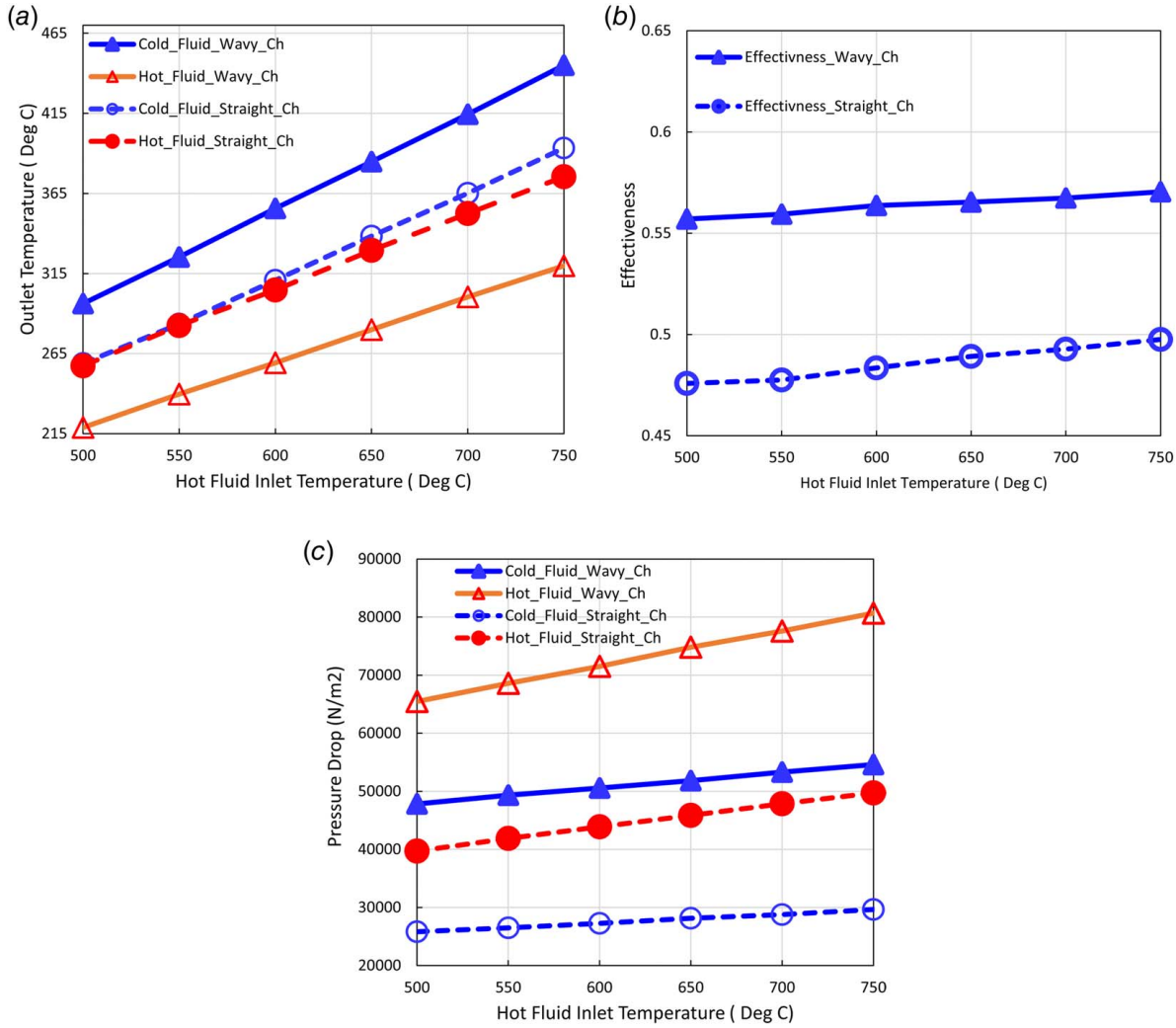

Fig. 15 Straight versus Wavy MCHE for hot temperature inlet DoE: (*a*) outlet temperatures, (*b*) effectiveness, and (*c*) straight versus wavy pressure drop for hot temperature inlet DoE

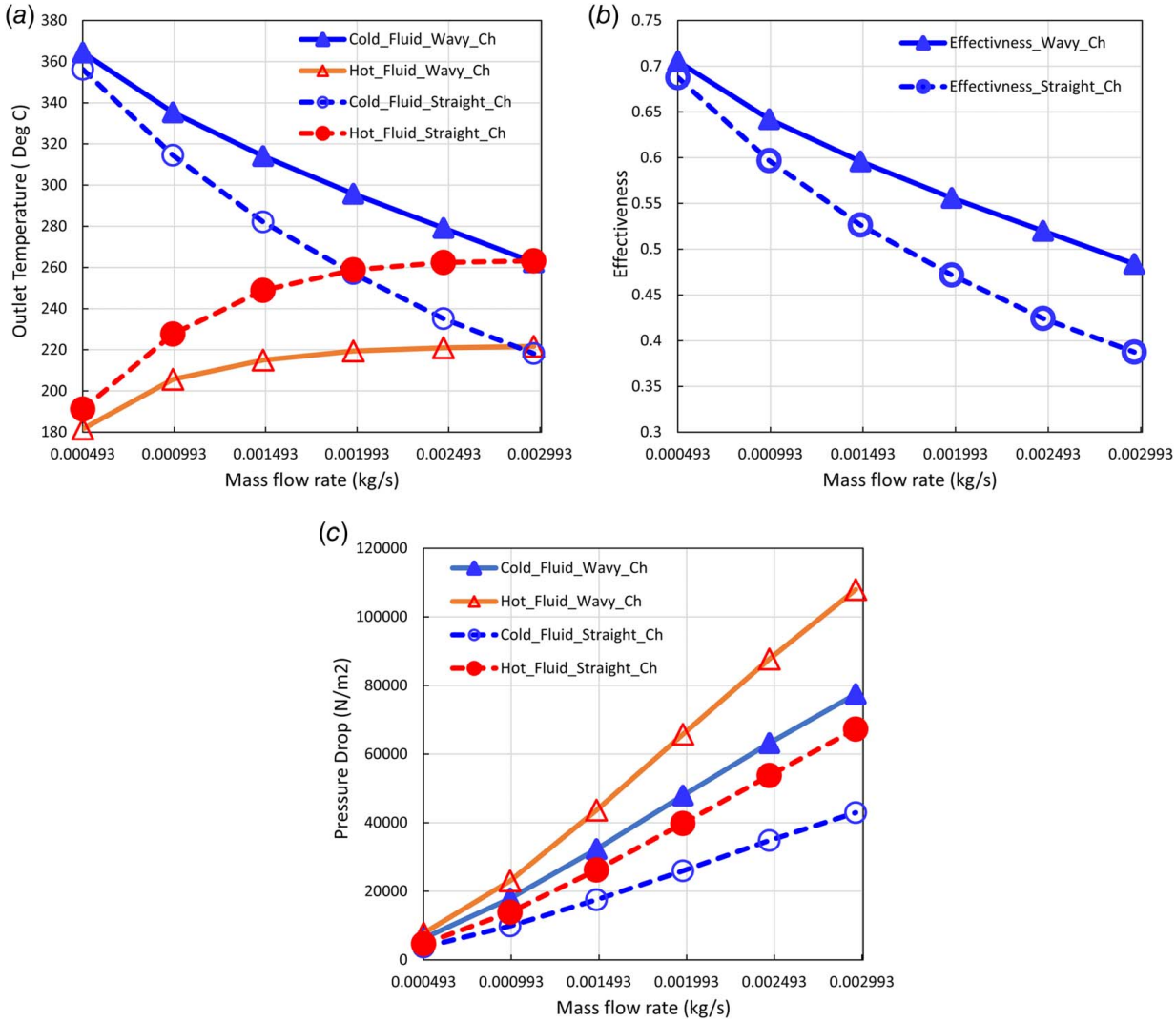

Fig. 16 Straight versus Wavy MCHE For balanced flow DoE: (*a*) outlet temperatures, (*b*) effectiveness, and (c) straight versus wavy pressure drop For balanced flow DoE

(a) Hot-fluid inlet temperature effect: When the results were compared for different materials under the same operating conditions, it was evident that a high longitudinal conducting material had high ineffectiveness and a high dimensionless longitudinal conduction parameter (λ).

Similarly, when the effectiveness of MCHE was plotted for the entire set of hot-fluid inlet temperatures DoE with and without considering longitudinal conduction effect, a drop of ~10%, ~4.5%, ~3.5%, and 2% in effectiveness was observed for Copper, Graphite, Silicon, and SST, as shown in Fig. 12(*a*).

(b) Balanced flow effect: When the results were compared for materials changed for balanced flow DoE for the same operating conditions, the results were in line with the physics, that is, high longitudinal conductivity leads to lower effectiveness of the MCHE. When balanced flow DoE was performed, it was concluded that a drop of ~16%, ~12%, 10.5%, and 6% in maximum MCHE effectiveness for Copper, Graphite, Silicon, and SST, respectively, was observed due to longitudinal conduction, as in Fig. 12(*b*).

The results obtained through the computational domain for material change for balanced flow and hot inlet temperature DoE for the same operating conditions validated the physics. Therefore, it was concluded that a high longitudinal conductivity increases the ineffectiveness of the MCHE.

The same computational model is also used to study the effect of anisotropic hypothetical Alumina (with thermal conductivity of 385 W/m-K across thickness and 22 W/m-K in other directions) on HTC and the effectiveness of MCHE and results are compared with isometric Alumina with thermal conductivity of 22 W/m-K for balanced flow scenarios. Results are shown in Figs. 13(*a*) and 13(*b*) It is concluded that anisotropic material-based MCHE sees ~1.2–2% higher HTC than isotropic Alumina MCHE for hot and cold fluid. Similarly, the effectiveness of anisotropic material-based MCHE is ~0.5–1.5% higher than isotropic Alumina MCHE for hot and cold fluids both. Therefore, it is recommended that for the best thermal performance of the MCHE, an anisotropic material with a very high thermal conductivity lateral (across thickness) and negligible in other directions should be used.

4 Performance Evaluation of Straight Channel Versus Wavy Channel MCHE

4.1 Model Description. A new computational 3D model of the MCHE was built using CFD-GEOM®, as described in Sec. 3, except for the channel geometry. The straight channel was replaced by a wavy channel of the same thickness, length, and width. All

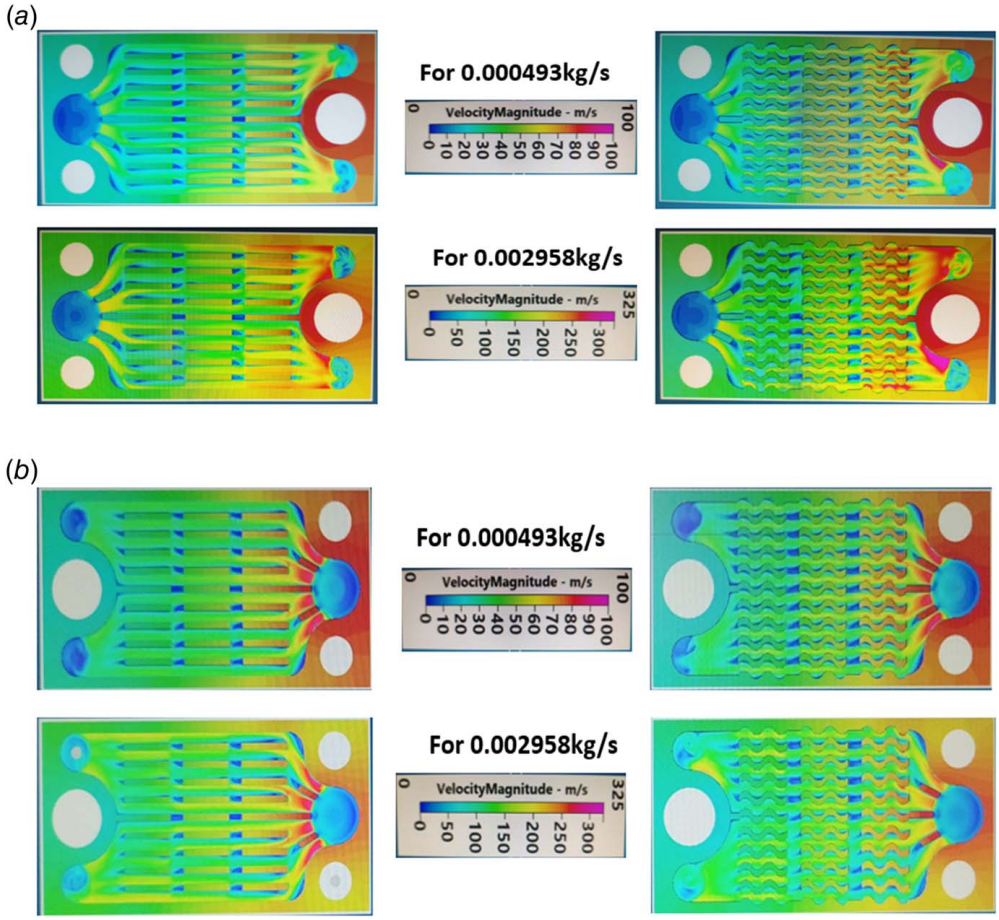

Fig. 17 (*a*) Velocity profile for cold fluid: (i) straight channel and (ii) wavy channel; (*b*) velocity profile for hot fluid: (i) straight channel and (ii) wavy channel

parameters were identical, except for the shape of the channel used as the reference design, as shown in Fig. 1. The geometry of the wavy channel is shown in Fig. 14.

The wavy channel has a longer travel path owing to a zig-zag path compared with the straight channel for the same straight length. Therefore, the fluid travel length in the straight channel from the inlet to the outlet was 14 mm, whereas it was 17 mm for the wavy channel for the same footprint. This extended travel in the zig-zag path in a wavy channel helped the fluid in more heat exchange as compared to a straight channel because of the longer residence time for the same footprint. However, the pressure drop also increased because of the torturous zig-zag path. Therefore, a trade-off between operating cost and performance is required to make the correct decision regarding its feasibility and applications.

4.2 Boundary Conditions. A new wavy channel design was also evaluated by performing the same detailed DoE using the same methodology followed during the validation stage for the identical scenarios as mentioned in Sec. 3.4 in this paper, for a straight channel MCHE for the same material. Later, the results of the wavy channel were compared with a straight channel for identical operating conditions.

4.3 Results and Discussion. The following conclusions were drawn when the performance of the new wavy channel design was compared with that of the existing straight channel design in terms of the pressure drop (ΔP) and effectiveness (ε) for the same and identical conditions.

(a) Hot-fluid inlet temperature effect: When this scenario was studied through a computational model of a new wavy channel MCHE with identical boundary conditions, it was observed that the hot fluid lost more heat and the cold fluid gained more heat than the straight channel configuration, that is, ∼15% more heat loss was observed in the hot fluid, whereas it was approximately 13% more heat gain for the cold fluid for the entire hot-fluid inlet temperature DoE, as shown in Fig 15(*a*). Approximately 17% greater effectiveness was predicted for the wavy channel configuration than for the straight channel configuration, as shown in Fig 15(*b*). Pressure drop is an essential factor that determines the power required to push the required flowrate in the MCHE. The friction factor is proportional to the pumping power. Therefore, the power consumption was increased by ∼85% and ∼63.5% in the wavy channel compared to the straight channel for cold and hot fluids, respectively, as shown in Fig 15(*c*).

(b) Balanced flow effect: When a balanced flow scenario was studied using the same computational model of a new wavy channel MCHE with identical boundary conditions, the wavy channel MCHE always performed better than the straight channel MCHE for the entire DoE with respect to the heat-transfer point of view. that is, ∼2% to 15% more heat loss was observed in the hot fluid, whereas it was ∼2% to ∼20% more heat gain for the cold fluid for the entire balanced flow DoE, as shown in Fig 16(*a*). ∼2.5% to ∼25% greater effectiveness was predicted for the wavy channel configuration than for the straight channel configuration, as shown in Fig 16(*b*).

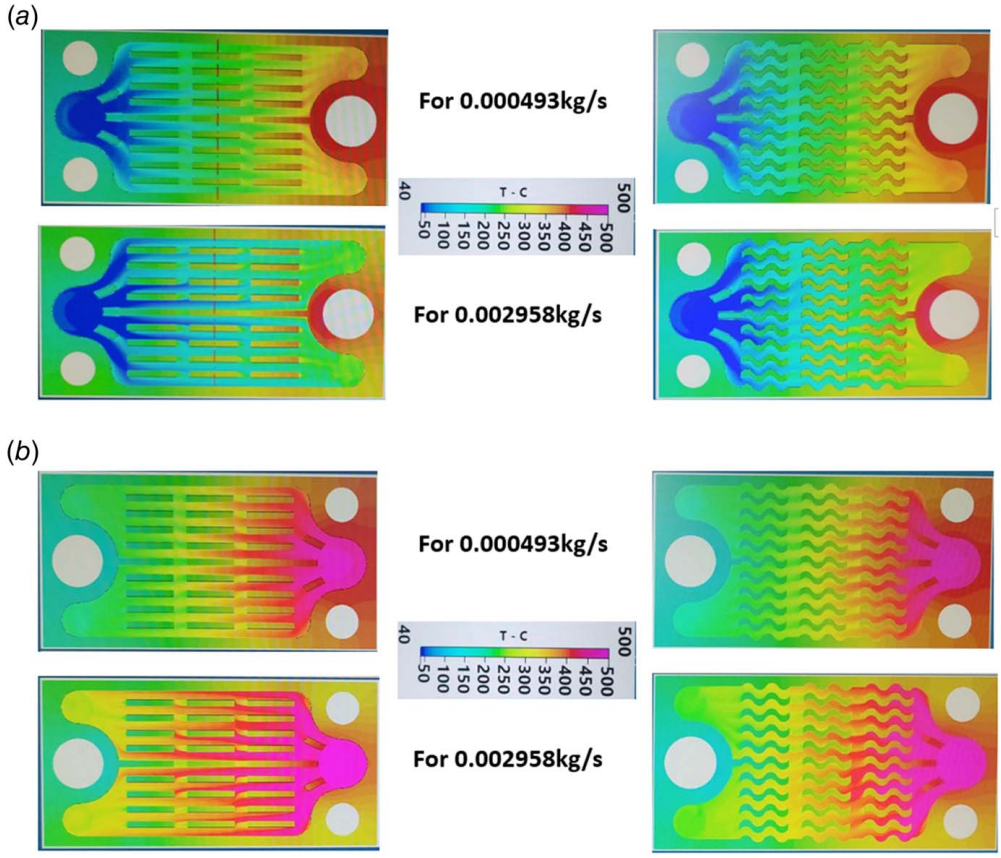

Fig. 18 (*a*) Temperature contour for cold fluid on the cold plate: (*i*) straight channel and (ii) wavy channel and (*b*) temperature contour for hot fluid on the hot plate: (i) straight channel and (ii) wavy channel

The performance of the wavy channel MCHE was almost the same as that of a straight channel MCHE at a lower flowrate because the primary heat-transfer mode was conduction instead of forced convection. As the flow increased, the convection mode started dominating the heat transfer, and the performance increased rapidly compared to that of the straight channel. Power consumption was also increased by ~85% and ~63.5% in wavy channels compared to the straight channel for cold and hot fluids, respectively, as shown in Fig 16(*c*), which is similar to what was observed in an earlier section.

The velocity contours for the hot and cold fluids are shown in Figs. 17(*a*) and 17(*b*) for the minimum and maximum flowrate scenarios, respectively, on the corresponding temperature-contoured plates. From the velocity contour in the flow channel, it was also concluded that the velocity of the hot fluid decreased from the inlet to the outlet as the density increased with a decrease in temperature owing to the energy heat exchange between the hot and cold fluids, and vice versa for the cold fluid.

At low flowrates, conduction dominates the convection mode. Therefore, the flow profiles and magnitudes in both configurations were similar. However, as the flow increased, convection dominated the heat transfer, and more heat transfer was observed compared with the straight channel.

Temperature contours are also shown for hot and cold fluids on the corresponding temperature-contoured plates for the minimum and maximum mass flowrates in Figs. 18(*a*) and 18(*b*). From the temperature contour of the fluid in the channel, it was also concluded that the cold fluid starts picking heat along the flow direction from the hot fluid as it moves from the inlet to the outlet and vice versa for the hot fluid.

(c) Unbalanced flow effect: When an unbalanced flow scenario was studied using the same computational model of a new wavy channel MCHE with identical boundary conditions, the results of the new hardware followed trends similar to those observed earlier for the entire DoE. i.e., ~7.5% to ~12% more heat loss was observed in hot fluid, whereas it was ~8% to ~15% more heat gain for cold fluid for the entire balanced flow DoE, as shown in Fig 19(*a*); ~10% to ~12% more effectiveness was predicted for the wavy channel configuration than for the straight channel configuration, as shown in Fig. 19(*b*).

The power consumption was still increased by ~85% and ~63.5% in the wavy channel compared to the straight channel for cold and hot fluids, respectively, as shown in Fig 19(*c*), which was similar to what was observed in an earlier section.

4.4 Performance Trade-Off Study. From this detailed comparative study, it was concluded that the thermal performance of the wavy channel MCHE is always higher than that of the straight channel MCHE. However, the pressure drop or pumping power needed to push the flow in the wavy channel MCHE is also very high compared with that in the straight channel MCHE. This indicates that if more thermal performance demands, one must go for wavy channels, and if pumping is critical, one must go for straight channels based on the pumping power available. For a clear understanding, a plot between the friction factor and heat-transfer coefficient (HTC) ratios is required. The Friction factors and HTCs for both hardware types (Straight and Wavy) were calculated using the following procedure, as mentioned using well-known correlations.

(1) Friction factor calculation (f): The friction factor was calculated using the following correlations for each case discussed

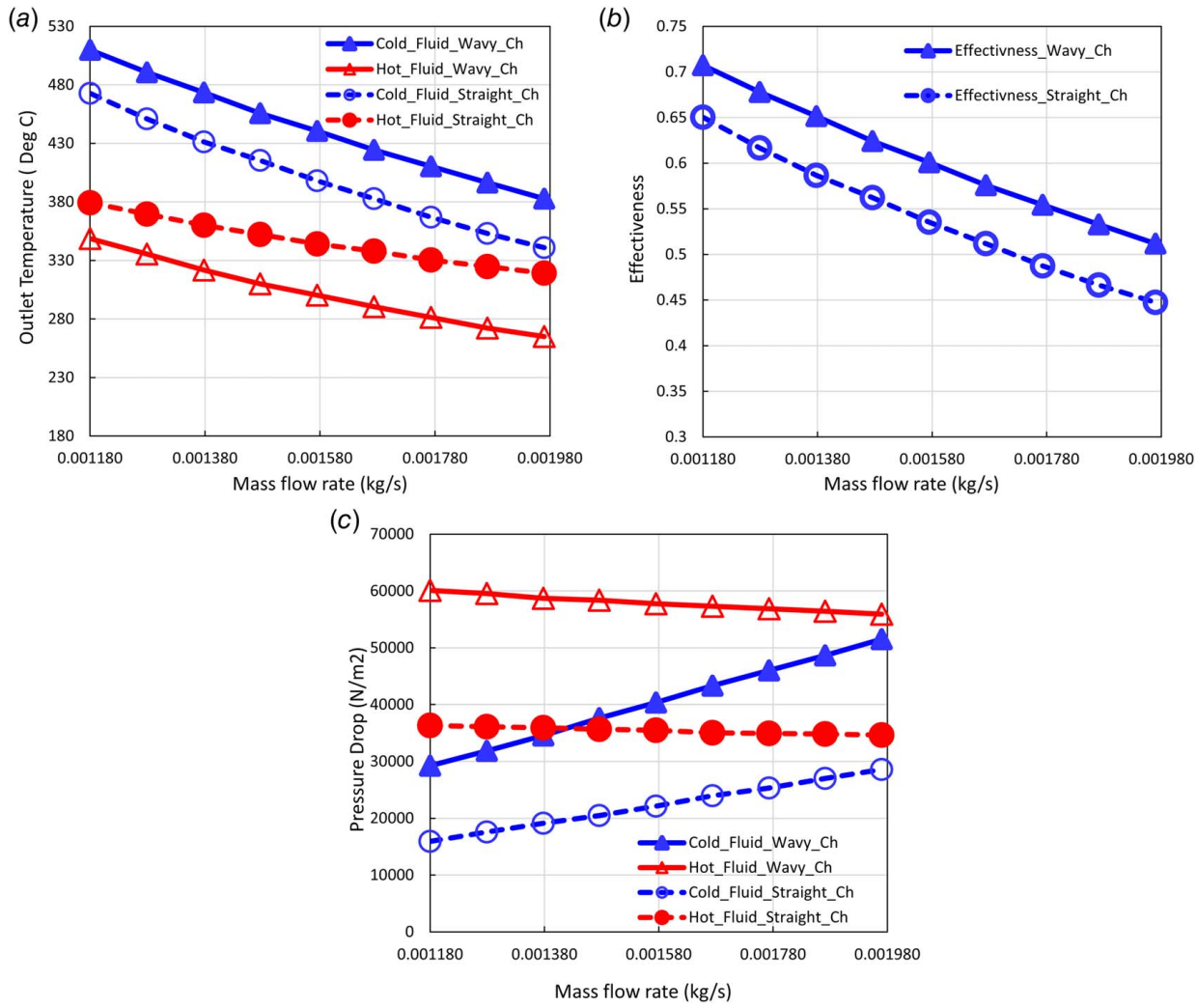

Fig. 19 Straight versus Wavy MCHE for unbalanced flow DoE: (*a*) Outlet Temperatures, (*b*) Effectiveness, and (c): Straight versus Wavy Pressure Drop for unbalanced flow DoE

in previous sections:

$$f = \frac{\Delta P}{\left(\frac{L}{d_i}\right)\left(\rho\frac{V^2}{2}\right)} \tag{12}$$

where ΔP is the pressure drop (N/m^2) across a single channel, L is the channel length (m), d_i is the hydraulic diameter of the circular channel (m), ρ is the fluid density (kg/m^3), and V is the fluid velocity (m/s).

(2) Temperature-dependent properties of the fluid and solids were used in the computational model. Therefore, various fluid properties, such as density, viscosity, specific heat, thermal conductivity, velocity, and pressure drop, were directly calculated from the computational model using area-weighted cell-centered values in the area of interest region from CFD-ACE® during postprocessing in CFD-VIEW®.

(3) Calculation of Nusselt number (Nu): The Nusselt Number was calculated for each case discussed in the previous sections using Dittus and Boelter's correlation [9].

$$\mathrm{Nu}_o = \frac{h_o D_h}{k} = 0.023\mathrm{Re}^{0.8}\,\mathrm{Pr}^n \tag{13}$$

where $n = 0.4$ for heating; $n = 0.3$ for cooling.

Then,

$$h_o = \frac{k}{D_h}\mathrm{Nu}_o \tag{14}$$

where D_h is the hydraulic diameter (m), h_o is the heat-transfer coefficient (HTC) in W/m^{2}K, k is the thermal conductivity of the fluid (W/m-K), Re is the Reynolds number $= \left(\frac{\rho VD}{\mu}\right)$, and μ is the dynamic viscosity (kg/m-s).

(4) The HTC and friction factor ratios for all sets were calculated using the following correlations:

$$\mathrm{HTC_}ratio = \mathrm{HTC}_{\mathrm{wavy}}/\mathrm{HTC}_{\mathrm{straight}} \tag{15}$$

$$f_ratio = f_{\mathrm{wavy}}/f_{\mathrm{straight}} \tag{16}$$

HTC_ratio versus f_ratio data are calculated and plotted for all DoEs as per the boundary conditions section. The HTC ratios and f_factor ratios are plotted as shown in Fig. 20 to understand variations of thermal performance and friction factors. This figure indicates that the increase in the friction factor is dominant (horizontal points) for the wavy channel compared to the HTC ratio.

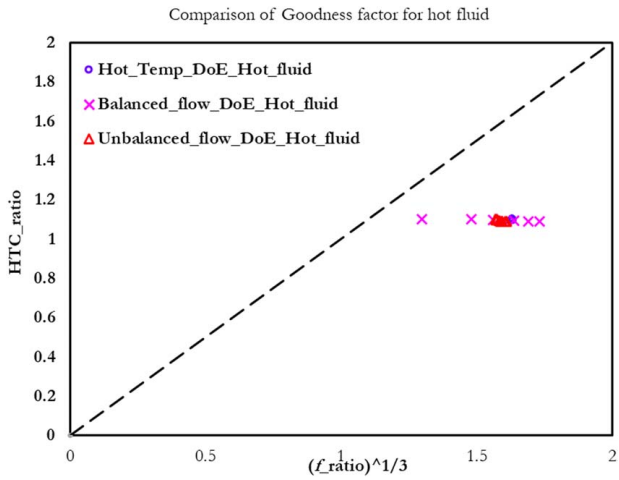

Fig. 20 Heat-transfer effectiveness versus pumping power for hot fluid for wavy

This numerical study clearly indicates that wavy channels are better for thermal performance, whereas straight channels are better for pumping power points of view. All points were under the cut-off line for this study. This implies that although the effectiveness is improved with a wavy channel, the power requirements dominate heat transfer. Therefore, this wavy channel MCHE is not suitable when the pumping power is critical or suitable for enhancing the heat-transfer coefficient.

The scope of future studies is still available with wavy channels, where the effect of the curvature of wavy channels can be studied to further reduce the friction factor and pumping power.

5 Conclusions

A detailed simulation study was carried out with validation of the computational model with experimental data published in the reference article and the setup discussed. The results are validated with experimental data with ~3–5% variation for hot fluid and ~6–12% for cold fluid for the entire design of experiments (DoEs). Further study was also carried out by applying a similar methodology for segmented wavy channel MCHE under identical conditions, and the results were compared with the same volume and area of the straight MCHE baseline design for various identical operating conditions. With the wavy channel MCHE, the performance in terms of effectiveness increased up to ~12–25% with respect to the straight MCHE. However, the pressure drop in the wavy channel MCHE also increased by ~60–80% under the same operating conditions as compared to the straight MCHE. Therefore, when heat-transfer coefficient enhancement is required, wavy channels are preferred, whereas straight channels are preferred for applications in which pumping power is the main factor. This numerical study provides information for the design of microchannel heat exchangers with straight and wavy channels, and their respective benefits. The effect of directional thermal conductivity is already shown in this paper. The heat exchanger material with the highest thermal conductivity will exhibit the least temperature drop across its thickness, resulting in higher surface temperatures on the cold fluid side. This will lead to increased heat transfer compared to isotropic materials. Additionally, the lowest thermal conductivity in the other direction will minimize heat loss through longitudinal conduction, enhancing the effectiveness of the heat exchanger. Therefore, it is recommended that for the best thermal performance of the MCHE, an anisotropic material with a very high thermal conductivity lateral (across thickness) and negligible in other directions should be used.

Acknowledgment

The authors wish to acknowledge the Birla Institute of Technology and Science (BITS), Pilani campus, Rajasthan, and Applied Materials® for carrying out Computational Fluid Dynamics (CFD) analysis and allowing the publication of this paper.

Conflict of Interest

There are no conflicts of interest.

Data Availability Statement

The datasets generated and supporting the findings of this article are obtainable from the corresponding author upon reasonable request.

Nomenclature

f = friction factor, dimensionless
h = heat-transfer coefficient, W/m^{2}K
k = thermal conductivity, W/m-k
m = mass, kg
L = distance between two inlet ports of hot and cold fluids, m
U = overall heat-transfer coefficient, W/m^{2}K
V = velocity of fluid, m/s
d_O = outer diameter, mm
d_i = hydraulic diameter of channel for ono-circular channel, m
h_{cold} = heat-transfer coefficient (HTC) for cold fluid, W/m^{2}K
h_{hot} = heat-transfer coefficient (HTC) for hot fluid, W/m^{2}K
k_{wall} = thermal conductivity of wall, W/m-K
A_c = longitudinal conduction cross-section area, m^2
A_s = convective surface area, m^2
C_{min} = minimum total heat capacity of fluid
D_h = hydraulic diameter, mm
Nu = Nusselt number, dimensionless
Pr = Prandtl number, dimensionless
Re = Reynolds number, dimensionless
St = Stanton number, dimensionless

Greek Symbols

ΔP = pressure drop, Pa
ε = effectiveness
$\acute{\varepsilon}$ = ineffectiveness
λ = dimensionless longitudinal conduction parameter
μ = viscosity, kg/m-s
ρ = density, kg/m^3

Subscripts

i = inner
o = outer

Abbreviations

CFD = computational fluid dynamics
DoE = design of experiment
HTC = heat-transfer coefficient
MCHE = microchannel heat exchangers
NTU = number of transfer units

References

[1] Dostal, V., 2004, "A Super Critical Carbon Dioxide Cycle," Ph.D. dissertation, Massachusetts Institute of Technology, Massachusetts, MA.
[2] Marchionni, M., Bianchi, G., and Tassou, S. A., 2020, "Review of Supercritical Carbon Dioxide (SCO2) Technologies for High-Grade Waste Heat to Power Conversion," SN Appl. Sci., **2**(4), pp. 1–13.

[3] Karayiannis, T. G., and Mahmoud, M. M., 2017, "Flow Boiling in Microchannels: Fundamentals and Applications," Appl. Therm. Eng., **115**, pp. 1372–1397.
[4] Uday Kumar, A., Javed, A., and Dubey, S. K., 2018, "Material Selection for Microchannel Heatsink: Conjugate Heat Transfer Simulation," IOP Conf. Ser.: Mater. Sci. Eng., **346**, p. 012024.
[5] Alm, B., Imke, U., Knitter, R., Schygulla, U., and Zimmermann, S., 2008, "Testing and Simulation of Ceramic Micro Heat Exchangers," Chem. Eng. J., **135**(S1), pp. 79–84.
[6] Kee, R. J., Almand, B. B., Blasi, J. M., Rosen, B. L., Hartmann, M., Sullivan, N. P., Zhu, H., et al., 2011, "The Design, Fabrication, and Evaluation of a Ceramic Counter-Flow Microchannel Heat Exchanger," Appl. Therm. Eng., **31**(11–12), pp. 2004–2012.
[7] Ionescu, V., and Neagu, A.-A., 2016, "Finite Element Method Analysis of a MEMS-Based Heat Exchanger With Different Channel Geometries," Energy Procedia, **112**, pp. 158–165.
[8] Ranganayakulu, C., Seetharamu, K. N., and Sreevatsan, K. V., 1997, "The Effects of Longitudinal Heat Conduction in Compact Plate-Fin and Tube-Fin Heat Exchangers Using a Finite Element Method," Int. J. Heat Mass Transfer, **40**(6), pp. 1261–1277.
[9] Kays, W. M., 1950, "Loss Coefficients for Abrupt Changes in Flow Cross Section With Low Reynolds Number Flow in Single and Multiple-Tube Systems," ASME J. Fluids Eng., **72**(8), pp. 1067–1074.
[10] McDonald, A. G., and Magande, H. L., 2012, *Fundamentals of Heat Exchanger Design*, John Wiley and Sons, Hoboken, NJ.
[11] Takeuchi, Y., Park, C., Noborio, K., Yamamoto, Y., and Konishi, S., 2010, "Heat Transfer in SiC Compact Heat Exchanger," Fusion Eng. Des., **85**(7–9), pp. 1266–1270.
[12] Fedorov, A. G., and Viskanta, R., 2000, "Three-Dimensional Conjugate Heat Transfer in the Microchannel Heat Sink for Electronic Packaging," Int. J. Heat Mass Transfer, **43**(3), pp. 399–415.
[13] Dang, T., Jyh-Tong, T., and Jiann-Cherng, C., 2010, "A Study on the Simulation and Experiment of a Microchannel Counter-Flow Heat Exchanger," Appl. Therm. Eng., **30**(14–15), pp. 2163–2172.
[14] Sheth, R. B., Stephan, R. A., and Hawkins-Reynolds, E., "Performance Characterization of a Microchannel Liquid/Liquid Heat Exchanger Throughout an Extended Duration Life Test," Proceedings of the 41st International Conference on Environmental Systems, 2011, Paper No. 5205.
[15] Hasan, M. I., Rageb, A. A., Yaghoubi, M., and Homayoni, H., 2009, "Influence of Channel Geometry on the Performance of a Counter Flow Microchannel Heat Exchanger," Int. J. Therm. Sci., **48**(8), pp. 1607–1618.
[16] Shakir, A. M., Mohammed, A. K., and Hasan, M. I., 2011, "Numerical Investigation of Counter Flow Microchannel Heat Exchanger With Slip Flow Heat Transfer," Int. J. Therm. Sci., **50**(11), pp. 2132–2140.
[17] Ramana Murthy, K. V., Ranganayakulu, C., and Ashok Babu, T. P., 2017, "Condensation Heat Transfer and Pressure Drop of R-134a Saturated Vapour Inside a Brazed Compact Plate Fin Heat Exchanger With Serrated Fin," Heat Mass Transfer, **53**(1), pp. 331–341.
[18] Chennu, R., 2018, "Numerical Analysis of Compact Plate-Fin Heat Exchangers for Aerospace Applications," Int. J. Numer. Methods Heat Fluid Flow, **28**(2), pp. 395–412.
[19] Jegan, C. D., and Azhagesan, N., 2018, "A Novel Investigation of Heat Transfer Characteristics in Rifled Tubes," Heat Mass Transfer, **54**(5), pp. 1503–1509.